8-18-2014

History and Dynamics of Net Rotation of the Mantle and Lithosphere

Maxwell L. Rudolph
Portland State University, rmaxwell@pdx.edu

Shijie Zhong
University of Colorado Boulder

Citation Details

Rudolph, M. L., and S. J. Zhong (2014), History and dynamics of net rotation of the mantle and lithosphere, Geochem. Geophys. Geosyst., 15, doi:10.1002/2014GC005457.

AGU PUBLICATIONS

Geochemistry, Geophysics, Geosystems

RESEARCH ARTICLE
10.1002/2014GC005457

Key Points:
- Net rotation history can be explained for past 25 Myr
- Rapid past net rotation requires new dynamical origin/revised reference frame
- Net rotation requires careful treatment in models incorporating plate motions

Supporting Information:
- Electronic Supplement
- Readme

Correspondence to:
M. L. Rudolph,
maxwell.rudolph@pdx.edu

Citation:
Rudolph, M. L., and S. J. Zhong (2014), History and dynamics of net rotation of the mantle and lithosphere, *Geochem. Geophys. Geosyst.*, *15*, doi:10.1002/2014GC005457.

Received 12 JUN 2014
Accepted 11 AUG 2014
Accepted article online 18 AUG 2014

History and dynamics of net rotation of the mantle and lithosphere

M. L. Rudolph[1,2] and S. J. Zhong[1]

[1]Department of Physics, University of Colorado, Boulder, Colorado, USA, [2]Now at Department of Geology, Portland State University, Portland, Oregon, USA

Abstract The net rotation of Earth's lithosphere with respect to the underlying mantle is the longest-wavelength component of toroidal flow in the mantle and is sensitive to both mantle buoyancy structure and lateral viscosity variations. The lithospheric net rotation in the geologic past implied by plate reconstructions using a hotspot reference frame for the past 100 Myr is up to five times greater than the present-day rate of lithospheric net rotation. We explore the role of lateral viscosity variations associated with subcontinental keels in producing the lithospheric net rotation for the geologic past and find that the introduction of subcontinental keels improves the agreement between modeled net rotation and the net rotation present in the plate reconstructions for the past 25 Myr. However, our models with continental keels produce at most 0.16°/Myr of differential rotation between the lithosphere and lower mantle for present-day, and explaining the most rapid rates of lithospheric net rotation during the Cretaceous and Paleogene remains challenging. This suggests the need for either an additional mechanism for generating lithospheric net rotation, or an adjustment to the absolute mantle reference frame relative to which plate motions are specified.

1. Introduction

Earth's past and present plate motions are a surface expression of convection in the underlying mantle. Plate motions provide a means to study the temporal evolution of mantle structure, which is linked to key present-day geophysical observables including the long-wavelength structure of the lower mantle, long wavelength geoid and spin axis orientation, the relative motions of plates, and the net rotation of the lithosphere. Plate motions are described relative to a reference frame, and all such reference frames for the recent geologic past are based on hotspot locations and relative motions. Geodynamic models that incorporate the kinematics of Earth's plate motion history provide an opportunity to explore the consistency of dynamically determined relative motions of the lithosphere and mantle with the plate motions determined relative to the hotspots or absolute mantle reference frame.

Any velocity field can be decomposed into toroidal and poloidal components, representing shearing/spinning and convergent/divergent motion, respectively. A significant amount of toroidal flow (related to deformation at transform plate boundaries, oblique convergence/divergence, and net rotation of the lithosphere) is one of the essential characteristics of Earth's present-day surface velocity field. Toroidal plate motion has attracted considerable interest in geodynamics, because its generation requires a special dynamic mechanism (e.g., lateral variations in mantle viscosity) [*Hager and O'Connell*, 1978] and also because the toroidal plate motion, unlike the poloidal plate motion, does not directly help transfer heat out of the Earth's mantle [*Olson and Bercovici*, 1991]. As the longest-wavelength toroidal component, the net rotation of the lithosphere is of particular interest because it is closely related to the reference frame relative to which plate motions are specified, but its origin is poorly understood [e.g., *Ricard et al*., 1991]. Determining the rate of net rotation requires a means to establish an absolute mantle reference frame and to distinguish between rigid rotation of the lithosphere and mantle together (true polar wander) and differential rotation between the mantle and lithosphere. Measurements of Earth's present-day net rotation rate range between 0.11 and 0.44°/Myr with typical reported uncertainties of ~25% or more. The higher estimates of net rotation relative to the hotspots, based on HS3B-MORVEL, favor a value ~0.34°/Myr [*Gripp and Gordon*, 2002; *Zheng et al*., 2010]. However, models of azimuthal seismic anisotropy produced by net rotation suggest that the observed seismic anisotropy is best explained by a net rotation rate <50% of the HS3 value

[*Becker*, 2008], SKS splitting observations suggest an upper bound of $<0.26^\circ$/Myr [*Conrad and Behn*, 2010], and trench migration rates also suggest less rapid net rotation [*Schellart et al*., 2008]. Comparable or even faster lithospheric net rotation may have occurred in the the past, as seen in plate motion history models for the last 120 Ma [*Lithgow-Bertelloni and Richards*, 1998] and 200 Ma [*Seton et al*., 2012], though the net rotation rates for the past are subject to larger uncertainties.

Lithospheric net rotation relative to the mantle can only be generated in buoyancy driven flows in the presence of lateral viscosity variations, perhaps related to high viscosity regions beneath continents [*Ricard et al*., 1991; *Zhong*, 2001; *Becker*, 2006] or related to the properties of slabs and plate boundaries [e.g., *Gérault et al*., 2012]. Plate motion history models [*Lithgow-Bertelloni and Richards*, 1998; *Seton et al*., 2012] have been used as time-dependent boundary conditions in convection models with different mantle viscosity structures to investigate the time evolution of mantle structures [e.g., *McNamara and Zhong*, 2005; *Zhang et al*., 2010; *Bower et al*., 2013]. However, lithospheric net rotation relative to the deep mantle is not necessarily present in these convection models, depending on mantle viscosity structure. By comparing the differential rotation between the lithosphere and lower mantle induced by plate motions with the net rotations relative to an absolute mantle reference frame as specified in the plate motion history models, we can test the validity of the assumed absolute mantle reference frame and the buoyancy and viscosity structure produced by our models. The optimal outcome of this test would be no net rotation of the lower mantle with respect to the absolute reference frame in which the plate motions are specified. We note that prior studies of net rotation have focused on understanding the present-day net rotation of the lithosphere by using free-slip or kinematic boundary conditions and exploring the mantle buoyancy and viscosity structure necessary to explain the lower estimates of present-day net rotation rate and pole location [*Ricard et al*., 1991; *Zhong*, 2001; *Becker*, 2006]. In our study, we obtain mantle buoyancy and viscosity structure through forward modeling in order to study the differential rotation between the lithosphere and mantle, focusing in particular on the rotation of the lower mantle relative to the absolute reference frame. This study has three parts. First, we examine the lithospheric net rotation present in surface velocity fields derived from two different plate motion models for the past 120–200 Myr [*Lithgow-Bertelloni and Richards*, 1998; *Seton et al*., 2012]. Second, we investigate the effects of plate motion models with different net rotation on mantle structure including the morphology of the Large Low Shear Velocity Provinces (LLSVPs) both for present day and for the past 200 Myr. Finally, we examine the lithospheric net rotation (relative to the lower mantle) present in our mantle convection simulations for both the present and the past and its dependence on mantle and lithospheric viscosity structures. We demonstrate that by incorporating differential viscous coupling between continental and oceanic plates with the underlying mantle, the history of differential rotation between the lithosphere and mantle is better reproduced.

2. Methods

We calculate the toroidal component of the surface velocity field, obtained from the radial component of the curl of the horizontal velocity field [e.g., *Lithgow-Bertelloni et al*., 1993]:

$$\left(\nabla\times\underline{v}(\theta,\phi)\right)\cdot\hat{\underline{e}}_r=\sum_{l=0}^{L}\sum_{m=0}^{l}V_l^m Y_l^m(\theta,\phi) \tag{1}$$

where $\underline{v}$ is the velocity field, Y_l^m is the spherical harmonic function at degree l and order m, V_l^m are the spherical harmonic coefficients for vorticity, θ is the longitude coordinate, ϕ is the colatitude coordinate, and $\hat{\underline{e}}_r$ is a unit vector in the outward radial direction. From the spherical harmonic coefficients V_l^m for vorticity, we compute the spherical harmonic amplitudes for toroidal velocities using $T_l^m=\frac{rV_l^m}{l(l+1)}$ [*Hager and O'Connell*, 1978; *Lithgow-Bertelloni et al*., 1993] where r is Earth's radius. We used CitcomS [*Zhong et al*., 2000, 2008] to compute the radial vorticity field from plate velocities and also used CitcomS to calculate toroidal spherical harmonic coefficients. We define the net rotation rate as $\underline{\omega}=\frac{3}{8\pi r^4}\int\underline{v}\times\underline{r}dS$ [*Torsvik et al*., 2010b; *Ricard et al*., 1991] and calculate net rotation rate and pole orientation from spherical harmonic coefficients using the method described in *Zhong* [2001, Appendix A].

We use primarily a recently developed plate reconstruction for the past 200 Myr by *Seton et al*. [2012] (S200 hereafter), exported from the GPlates software package [*Boyden et al*., 2011; *Gurnis et al*., 2012] at 1 Myr intervals for the kinematic analyses and convection modeling. Prior to 200 Myr, we use the proxy plate

reconstruction of *Zhang et al*. [2010] (Z450 hereafter) from 450 Ma until the first stage present in the reconstruction for the more recent geologic past. The Z450 proxy plate reconstruction was designed to incorporate Pangea assembly and breakup processeses from *Scotese* [2001] and transition smoothly to the first plate stage present in the plate reconstruction for the past 119 Myr by *Lithgow-Bertelloni and Richards* [1998] (LBR). We also present results from one calculation using Z450 and LBR as some previous studies of the evolution of mantle structures used either LBR alone [*McNamara and Zhong*, 2005] or Z450 and LBR [*Zhang et al*., 2010; *Zhang and Zhong*, 2011].

The plate motion history models are used in mantle convection models as time-dependent surface velocity boundary conditions, as done by *Zhang et al*. [2010]. Unless stated otherwise, we include an intrinsically dense layer in the lowermost mantle with a uniform initial thickness of 250 km, or ∼4.6% of the mantle by volume. While this initial volume is somewhat larger than estimates of LLSVP volume based on tomographic models [*Hernlund and Houser*, 2008], some entrainment of compositional tracers is unavoidable in numerical simulations, leading to slightly decreasing LLSVP volume over time. Our models are initialized with a radial temperature profile derived from a precalculation run to statistically steady state with free-slip boundary conditions in which the average surface velocity matches the average surface velocity at the earliest plate stage in the time-dependent velocity boundary conditions. We impose the first plate stage for 150 Myr prior to the start of the calculation with time-dependent plate boundary conditions at 458 Ma, the same procedure followed in *Zhang et al*. [2010]. The relative buoyancy of the intrinsically dense layer is described by the buoyancy ratio $B=\Delta\rho/(\rho_0\alpha\Delta T)$. Here, $\Delta\rho$ is the density difference between the chemically dense material and the ambient mantle, ρ_0 is the ambient mantle density, α is the thermal expansivity, and ΔT is the temperature difference between the surface and core-mantle boundary (CMB). We adopt a value of $B = 0.5$ in all cases, corresponding to a compositional density increase $\Delta\rho/\rho_0$ of 3.75%, assuming $\alpha=3\times10^{-5}\mathrm{K}^{-1}$ and $\Delta T=2500\mathrm{K}$ [e.g., *Zhang et al*., 2010]. We use temperature-dependent viscosity with temperature-dependence $\eta=\eta_0 \cdot \exp(E(0.5-T))$ where η is (dimensionless) viscosity, η_0 is a depth-dependent prefactor, E controls the temperature dependence, and T is dimensionless temperature, which varies between 0 at the surface and 1 at the CMB. The uppermost 150 km has a dimensionless viscosity prefactor of 1.0. We use a value of $E = 9.21$ leading to viscosity variations of 10^4 owing to temperature. There is a 30-fold viscosity prefactor decrease at 150 km depth and a 60-fold viscosity prefactor increase at 670 km depth. The depth-dependent prefactor increases linearly with depth from 670 km to the CMB with an overall factor of 3.4 increase. We show a representative viscosity profile for present day from Case 2 in Figure S1 (supporting information). We use a nominal Rayleigh number of $2.0 \cdot 10^8$ (defined using Earth's radius as characteristic length scale) for all cases. We used 64^3 elements on each of the 12 spherical caps in the CitcomS mesh, providing horizontal resolution of $\sim$ 102 km at the surface. Previous calculations with identical *Ra* and temperature-dependence of viscosity to those presented here were performed at both 12×48^3 and 12×64^3 resolution and found no significant differences [*Zhang et al*., 2010; *Zhang and Zhong*, 2011]. We summarize the parameters used in Table S1 (supporting information).

The relatively slow-moving continental plates and fast-moving oceanic plates may couple differently to the underlying mantle, and the difference in viscous coupling may play an important role in determining the differential rotation between the lithosphere and mantle [*Ricard et al*., 1991]. To better reproduce the differential rotation between the lithosphere and mantle, we explore the effect of continental keels, regions of higher viscosity beneath the continents that have been invoked in previous studies of present-day lithospheric net rotation [*Zhong*, 2001; *Becker*, 2006], which preferentially couple the continents to the underlying mantle. We use the surface age to define stable continental interiors, applying a continent/ocean function that labels the oldest fraction f of the surface "continent". We explored values of $f = 0.1$ and $f = 0.3$. This continent/ocean function is shown for the past 200 Myr in Figure S2 (supporting information). We introduce keels, regions of higher viscosity, underlying the continental regions identified with the continent/ocean function and extending to a fixed depth of 410 or 670 km (Cases 5 and 6). We assign a 10-fold viscosity increase to the keels, similar to values used in other studies in which continental and oceanic crust are coupled differentially to the underlying mantle [e.g., *Ricard et al*., 1991; *Zhong*, 2001; *Becker*, 2006]. The keels are implemented numerically by directly modifying the element viscosity in subcontinental regions. It should be emphasized that we do not think that the keels need to extend to 670 km or even 410 km depths to increase the coupling between the continents and the mantle for the Earth. The keels only need to extend beyond the asthenospheric depths ($< \sim 300$ km) to be effectively couple the keels to the deep

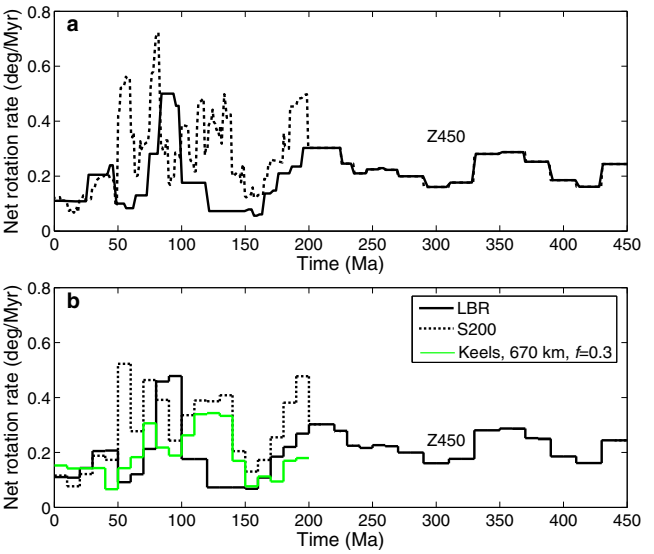

Figure 1. (a) Net rotation rates for the S200 and LBR plate motion models from 0 to 200 Ma and 0 to 119 Ma, respectively. Net rotation rate for Z450 is shown prior to 200 Ma. (b) Same as Figure 1a except averaged over 10 Myr intervals. We also show the differential rotation between the lithosphere and lower mantle from Case 6 (with continental keels extending to 670 km depth) also averaged over 10 Myr intervals in green.

mantle [e.g., *Zhong*, 2001]. Our mantle convection models do not consider a rheologically stratified asthenosphere-upper mantle viscosity structure, but rather have an uniformly weak upper mantle that extends to 670 km depth for simplicity, which is the reason for the keels to extend to 670 km depth to be effective.

3. Results

We first discuss the general characteristics of lithospheric net rotation in plate motion history models S200, LBR and Z450. The present-day rate of lithospheric net rotation in both the S200 and LBR plate reconstructions is 0.11°/Myr, as they are both based on standard relative plate motions for the present-day Earth in a hotspot reference frame. For the past 100 Myr, S200 uses the moving hotspot reference frame of [*O'Neill et al*., 2005]. Prior to 100 Ma, the S200 model uses a paleomagnetic reference frame, which is to say that it is assumed that Africa remains relatively stationary and other plates' motions are determined relative to Africa using apparent polar wander paths [*Torsvik et al*., 2008c]. LBR uses the fixed hotspot reference frame from *Gordon and Jurdy* [1986]. Net rotation rates vary significantly in the geologic past and differ between the two models (Figure 1). The maximum net rotation of 0.7–0.75°/Myr in the S200 model occurs around 80 Ma and the maximum net rotation of 0.5°/Myr in the LBR model occurs between 83 and 94 Ma, both of which are five to seven times greater than the present-day rate (Figure 1a). For the Z450 model before 120 Ma, the net rotation rates are generally smaller than 0.3°/Myr. However, the net rotation rates before 140 Ma are highly uncertain owing to very poorly constrained oceanic plate motions, and we will focus on the more recent net rotation rates in this study.

These plate motion models are used as time-dependent boundary conditions in convection models (Cases 1 and 2, Table 1). Case 1, using the combined Z450 and LBR models, is identical to case FS1 from *Zhang et al*. [2010] and case HF1 from *Zhang and Zhong* [2011], while Case 2 differs only in using Z450 and S200 plate motion models. Temporal evolution of mantle structure including LLSVPs for Case 1 was described in *Zhang et al*. [2010]. In Figure 2, we show the configuration of the LLSVP material for Cases 1 (brown outline) and 2 (shaded regions) at 50 Myr intervals from 200 Ma to the present. The LLSVP boundaries shown in Figure 2 are identified based on the nodal values of the composition field (tracked using tracers), and the shaded regions correspond to regions where the nodal composition $C \geq 0.5$ where LLSVP material has

Table 1. Summary of Simulations Discussed in the Text

Case Number	Plate Motions	$\eta_{0,LM}$	Rem Net Rot	LVVs?	Keel Fraction	Keel Depth (km)
1	Z450+LBR	2.0	N	Y		
2	Z450+S200	2.0	N	Y		
3	Z450+S200	1.0	N	Y		
4	Z450+S200	2.0	N	N		
5	Z450+S200	1.0	N	Y	0.3	410
6	Z450+S200	1.0	N	Y	0.3	670
7	Z450+S200	1.0	N	Y	0.1	670
8	Z450+S200	2.0	Global	Y		
9	Z450+S200	2.0	Mantle Only	Y		

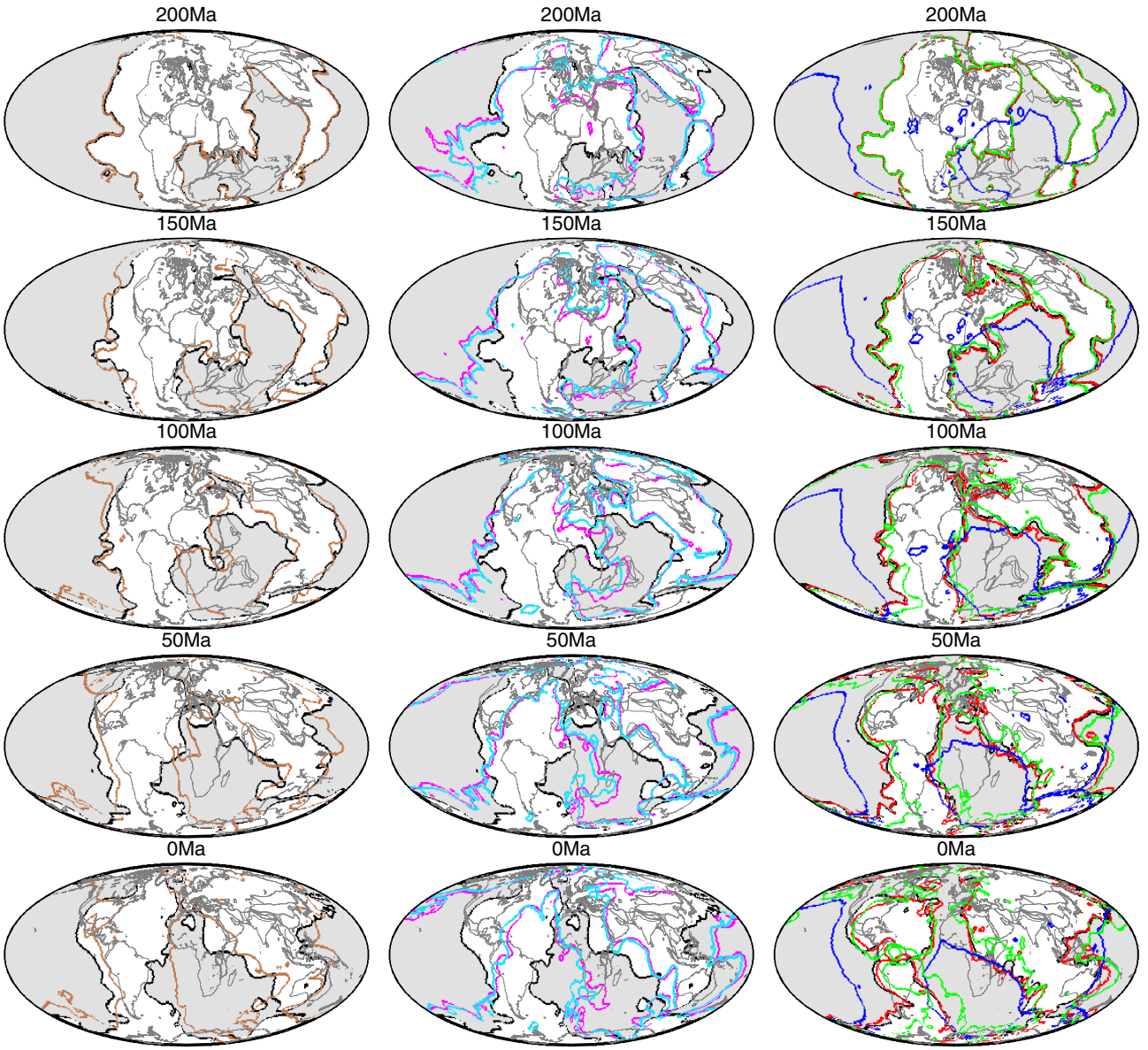

Figure 2. (left) Distribution of LLSVP material (gray regions) using the Z450+S200 plate motion models for Case 2 and LLSVP boundaries using the Z450+LBR plate motion models (Case 1, brown outline). (center) Effect of numerical treatment of net rotation on LLSVP boundaries. The gray shaded regions with black boundaries correspond to Case 2, in which the mantle was allowed to rotate freely. We also show LLSVP boundaries when the global net rotation is subtracted (purple, Case 8) and when the mantle net rotation is subtracted (turquoise, Case 9) [e.g., *Bower et al.*, 2013]. (right) Effect of continental keels on distribution of LLSVP material when there are lateral viscosity variations (LVVs) owing to temperature variations (grey regions, Case 3), when there are no keels and no LVVs (blue, Case 4), with keels extending to 410 km (red, Case 5), and with keels extending to 670 km (green, Case 6).

$C = 1$ and ambient mantle has $C = 0$. Prior to 200 Ma, both cases are identical. The S200 plate reconstruction (Case 2) produces present-day lower mantle structures that are shifted westward by 5°-10° relative to the structures produced using Z450 and LBR (Case 1). However, at long wavelengths, these two cases show similar lower mantle structures, including the dominantly degree-2 LLSVP structures for the present day. We will focus on lithospheric net rotation in this study and will not further contrast the mantle structures between these two cases with different plate motions.

The imposed surface net rotation $\underline{\omega}_{\text{surf}}$ from the plate motion models may induce some rotation $\underline{\omega}(r)$ of the underlying mantle, illustrated schematically in Figure 3. Ideally, if our models include all the essential physical processes and use adequate parameters, they would lead to a nonrotating mantle—there may be

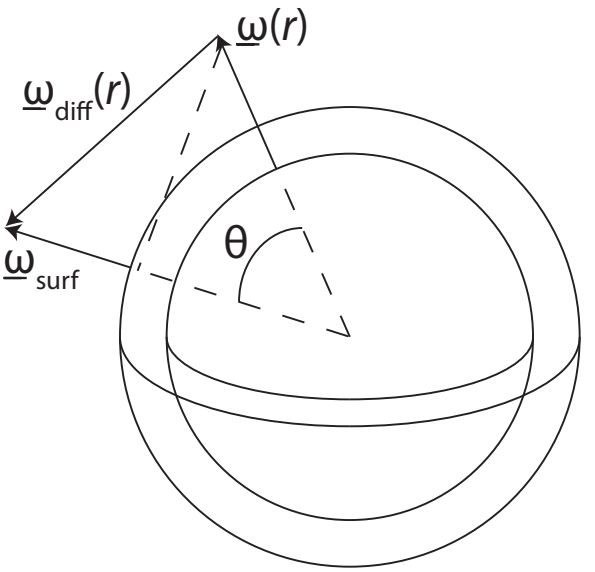

Figure 3. The coupling of surface net rotation ω_{surf} to net rotation at depth $\omega(r)$ is defined as $\hat{\omega}_{surf} \cdot \omega(r)/||\omega_{surf}||$. Geometrically, it is the projection of $\omega(r)$ onto ω_{surf} normalized by the surface net rotation rate. The separation of the net rotation vectors is shown by the angle θ.

differential rotation of the mantle relative to the lithosphere, but the net rotation of the mantle relative to the absolute reference frame in which the calculation is performed would be zero. In numerical models of mantle convection driven by velocity boundary conditions, net rotation of the mantle can be treated in at least three ways. These methods are designed to either preserve the dynamics of the interaction between the kinematically prescribed plate motions and mantle flow or to ensure that the net rotation of the lower mantle is kinematically consistent with the absolute mantle reference frame. First, the velocity boundary conditions can be applied as-is and the mantle may naturally rotate in response to any imposed net rotation. This approach was taken by *McNamara and Zhong* [2005], *Shephard et al*. [2012], and *Zhang et al*. [2010], and in Cases 1–7 discussed herein. Second, at each time step, the net rotation can be calculated globally and subtracted prior to advection of temperature and composition. This approach results in no net rotation of the mantle-lithosphere system as a whole, and results in the determination of velocities in a reference frame that is most appropriate for simulations in which the boundary conditions at the surface and core mantle boundary are free slip and hence the solution to the momentum equation is unaffected by arbitrary rigid body rotations [e.g., *Zhong et al*., 2008]. This approach is least appropriate for mantle convection simulations driven by kinematic boundary conditions because it results in mantle structure that may not be consistent with either the dynamics resulting from kinematically prescribed plate motions or the presumed fixity of the lower mantle relative to the absolute reference frame. A third approach is to calculate the net rotation of the mantle (excluding the lithosphere) induced by the imposed velocities and subtract this net rotation rate globally at each time step [*Bower et al*., 2013]. This approach guarantees that the imposed lithospheric net rotation is imposed as a differential rotation relative to the underlying mantle. Hence, the mantle as a whole will not rotate relative to the absolute mantle reference frame, but this comes at the expense of dynamical consistency.

In Figure 4 (top), we illustrate the effect of removing mantle net rotation schematically. In the bottom row, we show examples of downwelling structure (blue shaded regions) and LLSVP structures (red regions) at 98 Ma in models in which the lower mantle is allowed to rotate freely and in which the lower mantle's net rotation is calculated and removed globally (the method of *Bower et al*. [2013]). There is an apparent eastward migration of both downwellings and lower mantle thermal structures using the third [*Bower et al*., 2013] approach relative to the first approach. We show the morphology of the LLSVPs produced using each of the three approaches in Figure 2 (center column). In the three cases shown (Cases 2, 8 and 9), we use the S200 plate motion model and we vary only the method of net rotation treatment. At present day, the boundaries of both the African and Pacific LLSVPs in Cases 8 and 9, in which global and mantle net rotation are subtracted, are shifted up to $\sim 10-15^{\circ}$ northeast relative to the boundaries in Case 2, in which the mantle is allowed to rotate freely. Clearly, these calculations suggest that the method used to treat lithospheric net rotation significantly affects the predicted lower mantle structure by introducing relative rotation between the surface locations of plate boundaries and lower-mantle structures.

Differential rotation between the lithosphere and the mantle is sensitive to mantle viscosity structure (i.e., its lateral variations). To build intuition regarding the effect of mantle viscosity structure on differential rotation between the lithosphere and mantle, we performed a calculation (Case 4) without lateral viscosity variations (LVVs) using a horizontally averaged viscosity profile from Case 2. In the absence of LVVs, we expect any net rotation applied at the surface to couple perfectly with the underlying mantle [e.g., *Chandrasekhar*, 1961;

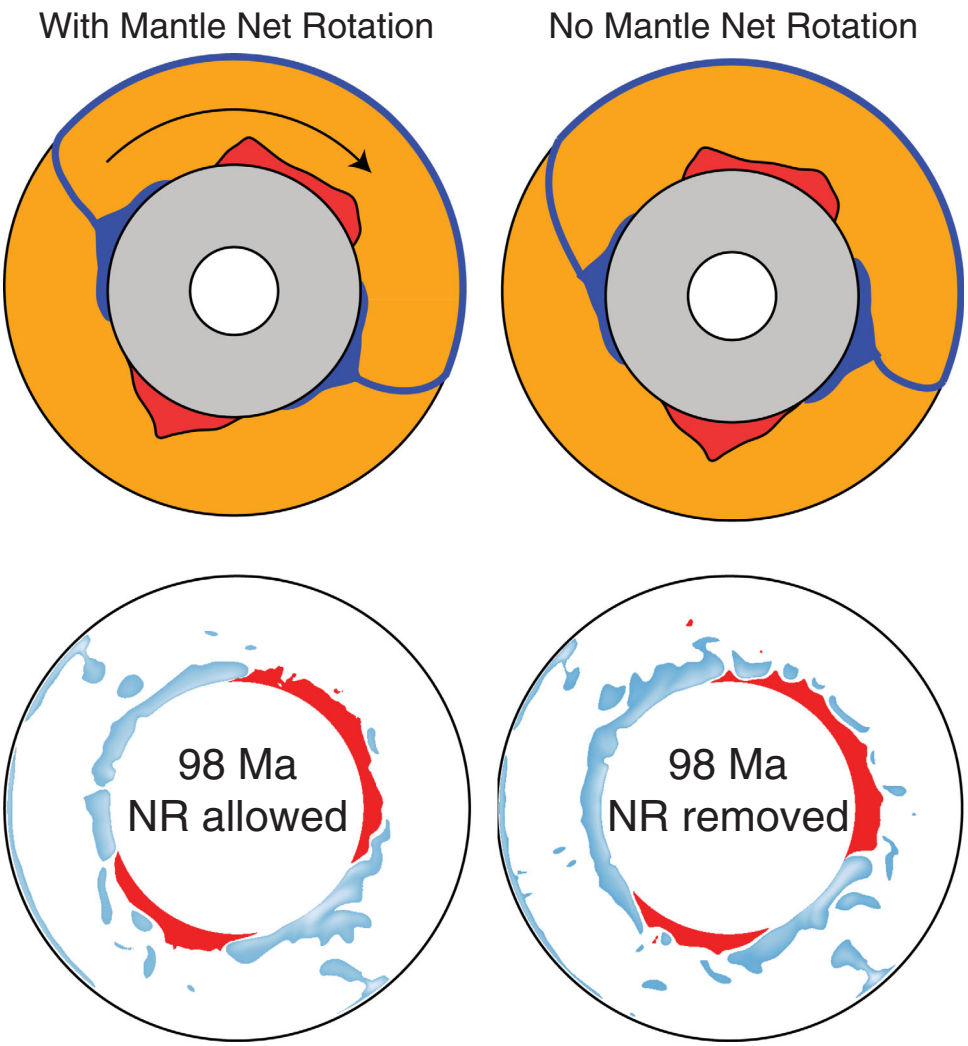

Figure 4. Effects of different approaches to treating net rotation on mantle thermal structure. (top) Schematic cartoons of equatorial slices of downwelling trajectories (blue) and LLSVP structure (red) in simulations where net rotation of the mantle is (left) allowed to occur and (right) removed at each time step. (bottom) Equatorial slices from 98 Ma from two of our numerical simulations in which mantle net rotation is (left) allowed (Case 2) and (right) removed at each time step (Case 9). We show cold anomalies (blue) and chemical pile structure (red). There is a net eastward (counter-clockwise) shift of the structures in the right column relative to those in the left column, indicating differing amounts of differential rotation between the lower mantle and the locations of convergent plate boundaries in the two simulations.

Hager and O'Connell, 1979, 1981], inducing a rigid body rotation (i.e., the mantle rotates together with the lithosphere). In Figure 5, we show the net rotation rate for the calculation without LVVs as a function of both depth and time (top row) and the angular separation between the surface net rotation vector $\underline{\omega}_{\text{surf}}$ and the interior net rotation $\underline{\omega}(r)$ (middle row). As expected, in the absence of lateral viscosity variations, the lithosphere and mantle rotate together, at the same rate and with zero angular separation (any departure from rigid rotation is due to numerical error). We also show a parameter R that we call the induced rotation (Figure 5, bottom), which is the projection of $\underline{\omega}(r)$ onto $\underline{\omega}_{\text{surf}}$, scaled by the surface net rotation rate ($R = \underline{\omega}(r) \cdot \hat{\underline{\omega}}_{\text{surf}} / ||\underline{\omega}_{\text{surf}}||$), illustrated schematically in Figure 3 (denotes a unit vector). The induced rotation represents the fraction of the imposed net rotation that is present at depth, and in the absence of LVVs, R is uniformly 1.0 (to within numerical error), as expected.

Next, we consider an otherwise identical case (Case 2) in which lateral viscosity variations arising from lateral temperature differences are allowed (Figure 5, middle). There is some differential rotation between the lithosphere and mantle, apparent in the variation of rotation rate with depth as well as the separation of the surface and interior rotation vectors. This differential rotation is accommodated by shear across a region

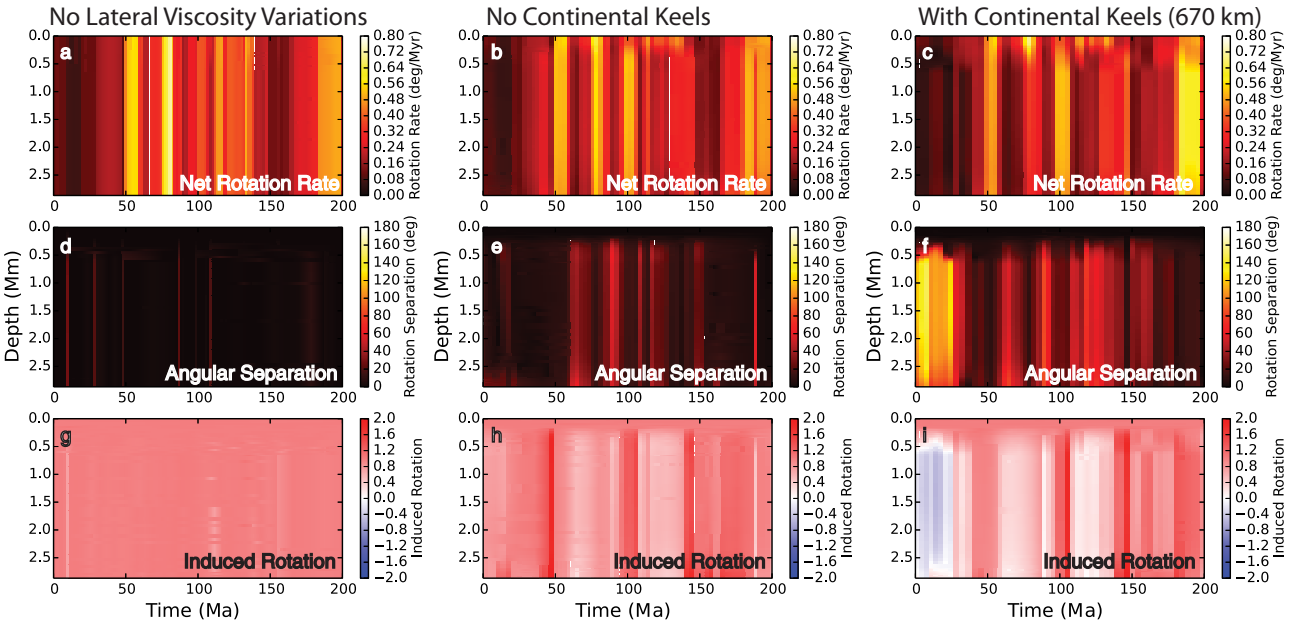

Figure 5. (a–c) Net rotation rate versus depth (vertical axis) and time (horizontal axis) from 200 Ma to present. (d–f) Separation of net rotation vector $\omega(r)$ from surface net rotation ω_{surf}. (g–i) Induced rotation (*R*, defined in text) of surface imposed net rotation to net rotation at depth. The left column corresponds to a case (Case 4) with only depth-dependent viscosity (i.e., no LVVs). The center column shows a case with no continental keels (Case 3), and the right column shows a scenario where we have included strong continental keels extending to the lower mantle and covering 3/10 of Earth's surface (Case 6).

extending from a depth of 150 km (the base of the lithosphere) to the lower mantle (670 km depth). In our models, the entire region from 150 to 670 km depth is relatively weak and has a uniform viscosity prefactor. The relatively strong lower mantle for the most part rotates coherently. Whereas in Case 4 with no lateral viscosity variations, the induced rotation *R* was uniform and equal to 1, for Case 2 with temperature-dependent viscosity the induced rotation decreases on average, though there are times when the induced rotation exceeds 1 (around 45 Ma and 145 Ma), meaning that the mantle rotates in the same direction but at a greater rate than the lithosphere. In Case 2, the angular separation between the surface and lower mantle rotation vectors rarely exceeds 20°, indicating that the lower mantle and lithosphere are generally rotating about a similar axis in the same direction. Clearly, this case with lateral variations in viscosity due to temperature alone does not produce a nonrotating mantle nor sufficient differential rotation between the lithosphere and the mantle as suggested by the plate motion model.

Cases 5 and 6 include additional lateral viscosity variations associated with viscous continental keels extending to depths of 410 and 670 km. Cases 5 and 6 were restarted from Case 2 at 200 Ma. Hence, Cases 2, 5, and 6 are identical at 200 Ma and diverge as time progresses. In Figure 5 (rightmost column) we show net rotation, pole separation, and induced rotation for Case 6 with $f = 0.3$ and keels extending to 670 km depth. In this case, the induced rotation is reduced further, becoming negative for the past 20 Myr, and the angular separation between the net rotation vectors for the surface and lower mantle exceeds 150°, implying that the mantle and lithosphere counter-rotate.

Figure 6a shows the rotation rate of the lower mantle for Cases 3–7, including cases with and without keels and LVVs. In general, larger values of *f* and deeper keels inhibit the lower mantle net rotation, though significant amounts of lower mantle net rotation still occur. Figure 6b shows the differential rotation between the surface and lower mantle, defined as the norm of the vector separating the surface and lower mantle rotation vectors ($||\underline{\omega}_{\text{surf}} - \underline{\omega}_{\text{lm}}||$, Figure 3). Larger values of differential rotation generally reflect a more stationary lower mantle. Here it is apparent that increasing *f* and the keel depth increases the differential rotation, as expected since lateral viscosity variations give rise to differential rotation. The depth to which the keels extend appears to have a much more significant effect than varying *f* in the range 0.1–0.3.

We show the LLSVP structures for cases without lateral viscosity variations (LVV)s, and with keels beneath continental areas (discussed later) extending to 410 and 670 km depth in Figure 2. Because the viscous

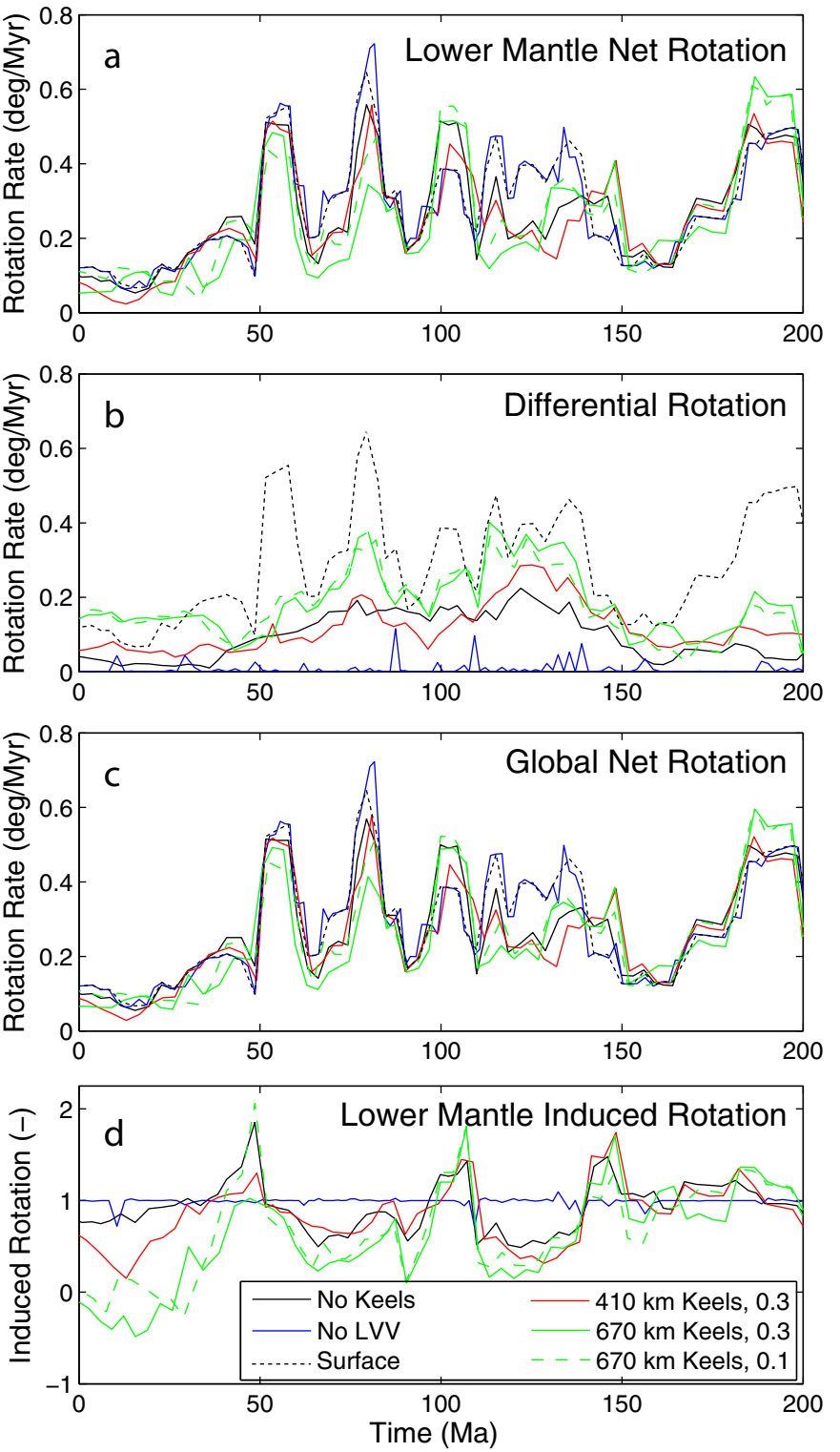

Figure 6. (a) Net rotation of the surface (black curve), and lower mantle (below 670 km depth) for cases with no keels (Case 3, red), keels extending to 410 km depth (Case 5, green) and to 670 km depth (Case 6, blue solid). (b) Same as above except showing differential rotation of the lower mantle relative to the lithosphere ($||\underline{\omega}_{surf} - \underline{\omega}_{lm}||$). Surface net rotation rate (black) is provided for reference. (c) Global net rotation (volume averaged $||\underline{\omega}(r)||$) for each case. (d) Dimensionless induced rotation R (defined in text) for each case.

continental keels affect the movement of the lower mantle relative to the locations of plate boundaries, the LLSVPs are shifted up to $\sim 10-15^{\circ}$ in the model with continental keels extending to 670 km depth (Case 6). When the keels extend only to 410 km depth, the LLSVP boundaries are very similar to those in Case 3, which is identical to Cases 5–7 except for the absence of keels. Case 4, which has no lateral viscosity variations has LLSVPs that remain degree-2 dominant from 200 Ma-present but which are less spatially extensive. The reduction in spatial extent is likely due in part to enhanced entrainment in the absence of a viscosity contrast between the LLSVP material and ambient mantle.

4. Discussion

Establishing a reference frame is one of the key steps in creating plate reconstructions. The choice of mantle reference frame for the present day is best understood, but the determination of even the present-day mantle reference frame is difficult. An absolute mantle reference frame like the one used in S200 is meant to represent a stationary lower mantle [e.g., *Čadek and Ricard*, 1992], which is in practice inferred for the recent past from hotspot locations and relative motions. Because there can be lateral motions in the lower mantle, the most logical choice for an absolute reference frame from a theoretical standpoint is one in which there is no net rotation of the lower mantle, and it is generally assumed that the mantle plumes supplying hot spots are the best existing proxy for this reference frame [e.g., *Wilson*, 1965; *Morgan*, 1971, 1972; *Solomon and Sleep*, 1974; *Doubrovine et al*., 2012]. Some absolute reference frames include corrections for true polar wander (TPW), re-orientation of the lithosphere-mantle system with respect to the spin axis, and by assumption geomagnetic dipole axis [e.g., *Steinberger and Torsvik*, 2008]. If not properly accounted for, TPW manifests itself in plate motions as a net rotation of the lithosphere, which can in principle introduce spurious differential rotation between the lithosphere and mantle, inconsistent with the definition of TPW as a rigid body rotation of the lithosphere and mantle together.

Net rotation of the lithosphere can in principle be driven by external (i.e., tidal) torques, or by lateral viscosity variations associated with differential viscous coupling between continental and oceanic plates with the underlying mantle (i.e., continental keels) [*Solomon and Sleep*, 1974; *Ricard et al*., 1991; *Zhong*, 2001; *Becker*, 2006] and with lateral viscosity variations associated with slabs and plate boundaries. Of these mechanisms, external torques can be ignored [*Jordan*, 1974]. *Gérault et al*. [2012] showed that in 2-D cylindrical-geometry simulations with free-slip boundary conditions, the rate of lithospheric net rotation depends more strongly on properties of slabs, the location of ridges, and the coupling of plates at the trench (i.e., presence and properties of a weak zone) and less strongly on the presence of continental keels. Our 3-D calculations use kinematically prescribed boundary conditions and consequently the locations and kinematics of plate boundaries, including trench migration, are not free parameters. Furthermore, because the kinematics of convergent plate boundaries are prescribed, the effect of weak zones in the lithosphere is unlikely to be important in generating net rotation in our models. The role of slabs in generating net rotation in 3-D spherical-geometry flow models may be more limited than the 2-D cylindrical geometry experiments of *Gérault et al*. [2012] suggest. *Becker and Faccenna* [2009] performed calculations in which lateral viscosity variations associated with slabs were incorporated using the slab model of *Steinberger* [2000] and found that the rate of net rotation produced by slabs was less than that produced in models that introduced continental keels, reaching only $\sim$10% of the HS3 rate. *Zhong* [2001] explored the influence of differences in coupling between continental and oceanic plates with the underlying mantle flow by varying the thickness of viscous continental keels. By imposing keels of up to 410 km thickness, *Zhong* [2001] achieved a maximum net rotation rate of 0.092°/Myr, close to the lower estimates of present-day net rotation. Lateral viscosity variations owing to a rheology with both temperature and stress-dependence can also explain the present-day net rotation [*Becker*, 2006]. Calculations using a stress and temperature-dependent rheology produce a predicted net rotation pole close to that of HS3-NUVEL1A and a net rotation rate of up to 99% of the value reported by *Gordon and Jurdy* [1986], even when the depth to which continental keels extend is $\sim$25% less than the 410 km used in *Zhong* [2001]. The maximum net rotation rates achieved by either *Zhong* [2001] or *Becker* [2006] are no more than $\sim 1/3$ of the net rotation in HS3B-MORVEL, $\sim 1/2$ the net rotation rate determined by either *Kreemer* [2009] based on SKS splitting or by *Becker* [2008] based on azimuthal anisotropy, and are much smaller than the maximum 10 Myr-averaged values present in the S200 velocity boundary conditions (0.53°/Myr) between 60 and 50 Ma.

In the more distant geologic past, determining net rotation becomes more difficult for three reasons. First, the lack of preserved oceanic crust leaves oceanic plate motions relatively unconstrained. By 150 Ma, $\sim$60% of

Earth's surface was covered by oceanic crust that has now been subducted, erasing the geologic record of plate motions [*Torsvik et al*., 2010b]. Oceanic plates move faster on average than continental plates and cover a greater fraction of Earth's surface and consequently can dominate the lithospheric net rotation. Second, the lack of preserved hotspot tracks makes it more difficult to obtain a proxy for an irrotational lower mantle reference frame. It has been suggested that the shapes of the LLSVPs have remained stationary for at least the past 200 Myr and possibly much longer, thus providing a possible mantle reference frame [*Torsvik et al*., 2008a, 2008b; *Domeier and Torsvik*, 2014]. The basis of this claim is the correlation between reconstructed large igneous province (LIP) eruption locations and the present-day margins of the LLSVPs [*Burke et al*., 2008; *Torsvik et al*., 2008a, 2010a]. Our mantle convection simulations indicate that the LLSVPs have remained dominantly degree-2 and relatively stationary for the past 150 Myr [*Zhang et al*., 2010] independent of which plate reconstruction is used for the imposed surface velocity boundary conditions (Figure 2). However, the duration of time over which the degree-2 LLSVP structures remain in a configuration similar to their present-day state remains unresolved [*Zhang et al*., 2010], and the robustness of the correlation between present-day LLSVP boundaries and the reconstructed LIP eruption locations may not support the use of present-day LLSVP boundaries as a constraint on LIP emplacement paleolongitude [*Austermann et al*., 2014].

In our numerical simulations that include continental keels, we find significant temporal variability of differential rotation between the lithosphere and mantle. Studies of present-day net rotation have been successful in reproducing the net rotation rate and orientation [*Zhong*, 2001; *Becker*, 2006]. Our models are most successful in producing the differential rotation between the lithosphere and mantle present in the S200 plate reconstruction for the past 50 Myr. In fact, for the past 25 Myr, the cases with keels extending to 670 km depth produce counter rotation of the lower mantle, indicated by the negative values of R (induced rotation) at lower mantle depths in Figure 5i as well as the angular separation of the rotation vector for lower mantle depths from the rotation vector for the lithosphere (Figures 5d–5f). The present-day rate of differential rotation in the calculations with continental keels is 0.06°/Myr with keels extending to 410 km depth (Case 5) and 0.16°/Myr for keels extending to 670 km depth (Case 6). The S200 model contains very large net rotation excursions between ~60-50 Ma and between 85- 75 Ma (Figure 6). None of our models with (or without) continental keels produce the differential rotation consistent with these values. There are several possible explanations for the disagreement: (1) the viscosity structure in our models does not adequately represent the coupling of the lithosphere with the lower mantle, (2) that the absolute reference frame used in the plate reconstruction includes a spurious net rotation, and (3) incorrect motions of (now subducted) oceanic plates.

Of these possibilities, (1) cannot be discounted, but the good agreement between the imposed net rotation rate and modeled differential rotation rate (Figures 1b and 6d) for the past c. 25 Myr suggests that our buoyancy and viscosity structure for this time period is reasonable and that it is likely to be reasonable for other times in the past where we see good agreement, for instance between 130 and 115 Ma. Possibility (2) deserves serious consideration. The absolute reference frame used in S200 for 100 Ma-present is a moving Indian/Atlantic hotspot reference frame from *O'Neill et al*. [2005], which accounts for relative motion of hotspots and the advection of plume conduits by mantle flow. The mantle flow field used in the reference frame determination is obtained using present-day density anomalies calculated from tomographic models together with time-dependent plate motions imposed as surface velocity boundary conditions taken from *Lithgow-Bertelloni and Richards* [1998] and *Gordon and Jurdy* [1986]. The models are run backward in time and heat is not allowed to diffuse. Because the flow field is calculated using a spectral method [*Hager and O'Connell*, 1979, 1981] that does not permit lateral viscosity variations [*Steinberger and O'Connell*, 1998, 2000], the flow field used to advect plume conduits cannot contain any differential rotation. As a result, any differential rotation that might naturally occur due to lateral viscosity variations cannot exist in these backward time-stepping calculations, similar to our case with no LVVs (Case 4, Figure 6b). In fitting hotspot tracks, *O'Neill et al*. [2005] do introduce lithospheric net rotations but in a way that is "artificial" [*Mihalffy et al*., 2008; *Doubrovine et al*., 2012] in the sense that the net rotations are not dynamically consistent with the model used for advecting plume conduits. Hence, the reference frame inferred based on hotspot motions may not adequately account for differential rotation between the lithosphere and lower mantle. Furthermore, it remains unclear how the simplified physics for plume dynamics in the backward-in-time mantle flow models by *Steinberger and O'Connell* [2000] which do not actually contain plumes, would affect lateral plume motions, as argued in *Zhong et al*. [2000] in which plume motions were tracked in fully dynamic models of the mantle. In addition to the potential pitfalls associated with the plume advection

calculations, the *O'Neill et al*. [2005] reference frame is based only on fitting hotspot tracks and age progressions in the African hemisphere and is not well suited to determining absolute plate motions in the Pacific hemisphere. This is particularly true prior to the formation of the Hawaii-Emperor bend c. 50 Ma, which is coincident with the episode of most rapid net rotation present in the S200 plate motion model (60-50 Ma). Plate motion models using reference frames established based on fitting hotspot tracks in both the African and Pacific hemisphere [*Torsvik et al*., 2010b; *Doubrovine et al*., 2012] generally yield smaller lithospheric net rotations than those present in S200 for 60-50 Ma. For instance, the net rotation between 60 and 50 Ma in the global moving hotspot reference frame GMHRF of *Doubrovine et al*. [2012] is 0.35°/Myr, much less than the rate of 0.53°/Myr present in S200 but still much greater than the differential rotation rate of 0.14°/Myr produced in Case 6 with keels extending to 670 km depth (Figure 1b). Despite having less rapid net rotation between 60 and 50 Ma than S200, GMHRF has somewhat higher net rotation for present-day, 0.19°/Myr, which slightly exceeds the maximum net rotation that we produce using continental keels (Case 6, 0.16°/Myr). The third possibility is difficult to quantify, but the magnitude of the effect is limited by the "world uncertainty", which is ∼30% at 50 Ma and ∼45% at 100 Ma [*Torsvik et al*., 2010b].

5. Conclusion

We analyzed the rate of lithospheric net rotation present in two plate motion models for the past 119–200 Myr (i.e., the LBR model by *Lithgow-Bertelloni and Richards* [1998] and S200 model by *Seton et al*. [2012]) and a proxy plate reconstruction extending to 450 Ma [*Zhang et al*., 2010]. The lithospheric net rotation rates contained in the plate motion models for the past 200 Myr are at times significantly higher than those at present. We performed several mantle convection simulations that incorporate high-viscosity continental keels, which act to better couple the slow-moving continental plates with the lower mantle. In general, our simulations with continental keels are more successful in reproducing the net rotation rates present in the S200 model than our simulations without keels, and the agreement between the imposed net rotation of the lithosphere and the resulting differential rotation between the lithosphere and lower mantle is particularly good for the past 25 Myr for cases with keels. However, the very large net rotation rates (>0.5°/Myr) during some periods of time in the S200 model are not well reproduced for any of the mantle viscosity structures that we considered. The resolution of this disagreement between imposed and modeled net rotation for the geologic past will require a better understanding of mantle rheology, further consideration of the methods used to establish an absolute mantle reference frame, and the extent to which plume locations in the lower mantle provide an adequate proxy for an absolute mantle reference frame.

Acknowledgments

We thank editor Thorsten Becker, reviewer Nicolas Flament, and two anonymous reviewers for their helpful comments which significantly improved this paper. This work was funded in part by the National Science Foundation through grants 1015669 and 1135382. This work utilized the Janus supercomputer, supported by the National Science Foundation (award CNS-0821794) and the University of Colorado Boulder as well as XSEDE allocation TG-EAR080022N through the Computational Infrastructure for Geodynamics (geodynamics.org). Figures were prepared using Generic Mapping Tools [*Wessel et al*., 2013] and matplotlib [*Hunter*, 2007]. Per the AGU Data Policy, all data required to reproduce the results described herein are available from the corresponding author upon request. CitcomS is available through the Computational Infrastructure for Geodynamics (geodynamics.org).

References

Austermann, J., B. T. Kaye, J. X. Mitrovica, and P. Huybers (2014), A statistical analysis of the correlation between large igneous provinces and lower mantle seismic structure, *Geophys. J. Int.*, *197*(1), 1–9, doi:10.1093/gji/ggt500.

Becker, T. W. (2006), On the effect of temperature and strain-rate dependent viscosity on global mantle flow, net rotation, and plate-driving forces, *Geophys. J. Int.*, *167*(2), 943–957.

Becker, T. W. (2008), Azimuthal seismic anisotropy constrains net rotation of the lithosphere, *Geophys. Res. Lett.*, *35*, L05303, doi:10.1029/2007GL032928.

Becker, T. W., and C. Faccenna (2009), A review of the role of subduction dynamics for regional and global plate motions, in *Subduction Zone Geodynamics*, edited by S. Lallemand and F. Funiciello, pp. 3–34, Springer, Heidelberg.

Bower, D. J., M. Gurnis, and M. Seton (2013), Lower mantle structure from paleogeographically constrained dynamic Earth models, *Geochem. Geophys. Geosyst.*, *14*, 44–63, doi:10.1029/2012GC004267.

Boyden, J. A., R. D. Müller, M. Gurnis, T. H. Torsvik, J. A. Clark, M. Turner, H. Ivey-Law, R. J. Watson, and J. S. Cannon (2011), Next-generation plate-tectonic reconstructions using GPlates, in *Geoinformatics: Cyberinfrastructure for the Solid Earth Sciences*, edited by G. R. Keller and C. Baru, pp. 95–113, Cambridge Univ. Press, Cambridge, U. K.

Burke, K., B. Steinberger, T. H. Torsvik, and M. A. Smethurst (2008), Plume generation zones at the margins of large low shear velocity provinces on the core–mantle boundary, *Earth Planet. Sci. Lett.*, *265*(1-2), 49–60.

Čadek, O., and Y. Ricard (1992), Toroidal/poloidal energy partitioning and global lithospheric rotation during Cenozoic time, *Earth Planet. Sci. Lett.*, *109*(3-4), 621–632.

Chandrasekhar, S. (1961), *Hydrodynamic and Hydromagnetic Stability, Int. Ser. of Monogr. on Phys.*, Oxford Univ. Press, Oxford, U. K.

Conrad, C. P., and M. D. Behn (2010), Constraints on lithosphere net rotation and asthenospheric viscosity from global mantle flow models and seismic anisotropy, *Geochem. Geophys. Geosyst.*, *11*, Q05W05, doi:10.1029/2009GC002970.

Domeier, M., and T. H. Torsvik (2014), Plate tectonics in the late Paleozoic, *Geosci. Frontiers*, *5*(3), 303–350.

Doubrovine, P. V., B. Steinberger, and T. H. Torsvik (2012), Absolute plate motions in a reference frame defined by moving hot spots in the Pacific, Atlantic, and Indian oceans, *J. Geophys. Res.*, *117*, B09101, doi:10.1029/2011JB009072.

Gérault, M., T. W. Becker, B. J. P. Kaus, C. Faccenna, L. Moresi and L. Husson (2012), The role of slabs and oceanic plate geometry in the net rotation of the lithosphere, trench motions, and slab return flow, *Geochem. Geophys., Geosyst.*, *13*, Q04001, doi:10.1029/2011GC003934.

Gordon, R. G., and D. M. Jurdy (1986), Cenozoic global plate motions, *J. Geophys. Res.*, *91*, 12,389–12,406.

Gripp, A. E., and R. G. Gordon (2002), Young tracks of hotspots and current plate velocities, *Geophys. J. Int.*, *150*(2), 321–361.
Gurnis, M., M. Turner, S. Zahirovic, L. DiCaprio, S. Spasojevic, R. D. Müller, J. Boyden, M. Seton, V. C. Manea, and D. J. Bower (2012), Plate tectonic reconstructions with continuously closing plates, *Comput. Geosci.*, *38*(1), 35–42.
Hager, B. H., and R. J. O'Connell (1978), Subduction zone dip angles and flow driven by plate motion, *Tectonophysics*, *50*(2–3), 111–133.
Hager, B. H., and R. J. O'Connell (1979), Kinematic models of large-scale flow in the Earth's mantle, *J. Geophys. Res.*, *84*, 1031–1048.
Hager, B. H., and R. J. O'Connell (1981), A simple global model of plate dynamics and mantle convection, *J. Geophys. Res.*, *86*, 4843–4867.
Hernlund, J. W., and C. Houser (2008), On the statistical distribution of seismic velocities in Earth's deep mantle, *Earth Planet. Sci. Lett.*, *265*(3–4), 423–437.
Hunter, J. D. (2007), Matplotlib: A 2D graphics environment, *Comput. Sci. Eng.*, *9*(3), 90–95.
Jordan, T. H. (1974), Some comments on tidal drag as a mechanism for driving plate motions, *J. Geophys. Res.*, *79*, 2141–2142.
Kreemer, C. (2009), Absolute plate motions constrained by shear wave splitting orientations with implications for hot spot motions and mantle flow, *J. Geophys. Res.*, *114*, B10405, doi:10.1029/2009JB006416.
Lithgow-Bertelloni, C., and M. A. Richards (1998), The dynamics of Cenozoic and Mesozoic plate motions, *Rev. Geophys.*, *36*, 27–78.
Lithgow-Bertelloni, C., M. A. Richards, Y. Ricard, R. J. O'Connell and D. C. Engebretson (1993), Toroidal-poloidal partitioning of plate motions since 120 MA, *Geophys. Res. Lett.*, *20*, 375–378.
McNamara, A. K., and S. Zhong (2005), Thermochemical structures beneath Africa and the Pacific Ocean, *Nature*, *437*(7062), 1136–1139.
Mihalffy, P., B. Steinberger, and H. Schmeling (2008), The effect of the large-scale mantle flow field on the Iceland hotspot track, *Tectonophysics*, *447*(1-4), 5–18.
Morgan, W. J. (1971), Convection plumes in the lower mantle, *Nature*, *230*(5288), 42–43.
Morgan, W. J. (1972), Deep mantle convection plumes and plate motions, *AAPG Bull.*, *56*(2), 203–213.
Olson, P., and D. Bercovici (1991), On the equipartition of kinetic energy in plate tectonics, *Geophys. Res. Lett.*, *18*, 1751–1754.
O'Neill, C., D. Müller, and B. Steinberger (2005), On the uncertainties in hot spot reconstructions and the significance of moving hot spot reference frames, *Geochem. Geophys. Geosyst.*, *6*, Q04003, doi:10.1029/2004GC000784.
Ricard, Y., C. Doglioni, and R. Sabadini (1991), Differential rotation between lithosphere and mantle: A consequence of lateral mantle viscosity variations, *J. Geophys. Res.*, *96*, 8407–8415.
Schellart, W. P., D. R. Stegman, and J. Freeman (2008), Global trench migration velocities and slab migration induced upper mantle volume fluxes: Constraints to find an Earth reference frame based on minimizing viscous dissipation, *Earth Sci. Rev.*, *88*(1–2), 118–144.
Scotese, C. R. (2001), Atlas of Earth history, *Tech. Rep. 90–0497*, Arlington, Tex.
Seton, M., et al. (2012), Global continental and ocean basin reconstructions since 200 Ma, *Earth Sci. Rev.*, *113*(3–4), 212–270.
Shephard, G. E., H. P. Bunge, B. S. A. Schuberth, R. D. Müller, A. S. Talsma, C. Moder, and T. C. W. Landgrebe (2012), Testing absolute plate reference frames and the implications for the generation of geodynamic mantle heterogeneity structure, *Earth Planet. Sci. Lett.*, *317–318*, 204–217.
Solomon, S. C., and N. H. Sleep (1974), Some simple physical models for absolute plate motions, *J. Geophys. Res.*, *79*, 2557–2567.
Steinberger, B. (2000), Slabs in the lower mantle—Results of dynamic modelling compared with tomographic images and the geoid, *Phys. Earth Planet. Inter.*, *118*(3–4), 241–257.
Steinberger, B., and R. J. O'Connell (1998), Advection of plumes in mantle flow: Implications for hotspot motion, mantle viscosity and plume distribution, *Geophys. J. Int.*, *132*(2), 412–434.
Steinberger, B., and R. J. O'Connell (2000), Effects of mantle flow on hotspot motion, in *The History and Dynamics of Global Plate Motions*, edited by M. A. Richards, R. G. Gordon, and R. D. van der Hilst, pp. 377–398, AGU, Washington, D. C.
Steinberger, B., and T. H. Torsvik (2008), Absolute plate motions and true polar wander in the absence of hotspot tracks, *Nature*, *452*(7), 620–623.
Torsvik, T., M. Smethurst, K. Burke, and B. Steinberger (2008a), Long term stability in deep mantle structure: Evidence from the 300 Ma Skagerrak-Centered Large Igneous Province (the SCLIP), *Earth Planet. Sci. Lett.*, *267*(3-4), 444–452.
Torsvik, T., B. Steinberger, L. Cocks, and K. Burke (2008b), Longitude: Linking Earth's ancient surface to its deep interior, *Earth Planet. Sci. Lett.*, *276*(3-4), 273–282.
Torsvik, T. H., R. D. Müller, R. Van der Voo, B. Steinberger, and C. Gaina (2008c), Global plate motion frames: Toward a unified model, *Rev. Geophys.*, *46*, RG3004, doi:10.1029/2007RG000227.
Torsvik, T. H., K. Burke, B. Steinberger, S. J. Webb, and L. D. Ashwal (2010a), Diamonds sampled by plumes from the core-mantle boundary, *Nature*, *466*(7304), 352–355.
Torsvik, T. H., B. Steinberger, M. Gurnis, and C. Gaina (2010b), Plate tectonics and net lithosphere rotation over the past 150 My, *Earth Planet. Sci. Lett.*, *291*(1–4), 106–112.
Wessel, P., W. H. F. Smith, R. Scharroo, J. Luis, and F. Wobbe (2013), Generic mapping tools: Improved version released, *Eos Trans. AGU*, *94*(45), 409–410.
Wilson, J. T. (1965), Evidence from ocean islands suggesting movement in the Earth, *Philos. Trans. R. Soc. London A*, *258*(1088), 145–167.
Zhang, N., and S. Zhong (2011), Heat fluxes at the Earth's surface and core–mantle boundary since Pangea formation and their implications for the geomagnetic superchrons, *Earth Planet. Sci. Lett.*, *306*(3–4), 205–216.
Zhang, N., S. Zhong, W. Leng, and Z.-X. Li (2010), A model for the evolution of the Earth's mantle structure since the Early Paleozoic, *J. Geophys. Res.*, *115*, B06401, doi:10.1029/2009JB006896.
Zheng, L., R. G. Gordon, C. Kreemer, C. DeMets, and D. F. Argus (2010), Current plate motions relative to the hotspots consistent with the MORVEL global set of plate relative angular velocities, *EGU Gen. Assem. Conf. Abstr.*, *12*, EGU2010-14191.
Zhong, S. (2001), Role of ocean-continent contrast and continental keels on plate motion, net rotation of lithosphere, and the geoid, *J. Geophys. Res.*, *106*, 703–712.
Zhong, S., M. T. Zuber, L. Moresi, and M. Gurnis (2000), Role of temperature-dependent viscosity and surface plates in spherical shell models of mantle convection, *J. Geophys. Res.*, *105*, 11,063–11,082.
Zhong, S., A. McNamara, E. Tan, L. Moresi, and M. Gurnis (2008), A benchmark study on mantle convection in a 3-D spherical shell using CitcomS, *Geochem. Geophys. Geosyst.*, *9*, Q10017, doi:10.1029/2008GC002048.